Experimental investigation of turbulent flows through a boulder array placed on a permeable bed

Hui Cao, Chen Ye, Xu-Feng Yan, Xing-Nian Liu and Xie-Kang Wang

ABSTRACT

Glass beads were used to model permeable beds and boulders (simulated by plastic spherical balls) placed on the centre section of the bed. Flume experiments were conducted to investigate the hydrodynamics through a boulder array over impermeable and permeable beds (i.e. IMPB and PB). For background reference, hydrodynamics investigation was made over smooth beds (SB) with the boulder array. Through measuring the instantaneous velocity field, the major flow characteristics such as mean flow velocity, turbulence intensity, turbulent kinetic energy (TKE) and instantaneous Reynolds stresses (through quadrant analysis) were presented. The results show that the increase in bed permeability through decreasing the exposure height of boulders has little impact on the magnitude of streamwise velocity, but tends to decrease the near-bed velocity gradient, thus affecting the bed shear-stress. For turbulence, similar to the previous studies, the bed permeability is identified to enable a downward shift of the peak of turbulence intensity. The TKE budget analysis shows that bed permeability tends to inhibit the transport and diffusion processes of TKE generation. Finally, the quadrant analysis of turbulence structure clearly shows that the ejections ($Q2$) and sweeps ($Q4$) with and without the boulder array are dominated by turbulence structure of different scales.

Key words | bed permeability, boulder array, TKE budget, turbulence bursting, wall-bounded flows

Hui Cao
Xu-Feng Yan
Xing-Nian Liu
Xie-Kang Wang (corresponding author)
State Key Laboratory of Hydraulics and Mountain River Engineering,
Sichuan University,
Chengdu 610065,
China
E-mail: *wangxiekang@scu.edu.cn*

Hui Cao
China Three Gorges Corporation,
Beijing 100038,
China
and
Three Gorges Cascade Dispatching Communication Center,
Chengdu 610041, Sichuan,
China

Chen Ye
College of Harbour and Environmental Engineering,
Jimei University,
Xiamen 361000,
China

INTRODUCTION

In mountain rivers, immobile boulders are regarded as large bed obstacles, largely influencing the spatial and temporal variability in flow and topographic dynamics (Euler *et al.* 2017; Afzalimehr *et al.* 2019). The investigation of the effects of boulders on flow structures is difficult to perform due to the complexity of the bed surface geometry configuration. Many laboratory studies focused on the mean and turbulent flow characteristics in their vicinity and the complex eddy structures around boulders (e.g. Shamloo *et al.* 2001; Sadeque *et al.* 2009; Dey *et al.* 2011). Regarding an isolated boulder, it is found that three different regions can be identified along the centre line of the boulder, including downstream of the boulder, an intermediate region and upstream of the boulder. For the downstream region of a boulder, the velocity profile appears to be complex over the entire flow depth and a near-wake region forms when flow separates at the edge of the boulder, resulting in downstream flow recirculation. Meanwhile, a far-wake region beyond the near-wake region enables flow to return to a normal state near the bed as upstream. In real situations, boulders in mountain streams commonly occur in arrays. Particularly, multiple arrays of isolated boulders in a regular

doi: 10.2166/ws.2020.046

staggered pattern can be observed in mountain streams (e.g. Lawless & Robert 2001; Papanicolaou *et al.* 2012).

In terms of turbulent flow characteristics solely past a boulder array, researchers point out that flows around an individual boulder in an array, different from those around an isolated one, are impacted by flow retardation and backwater effects upstream of the array. Therefore, flow structure around an individual boulder would be largely modified in comparison with the isolated-boulder configuration. Baki *et al.* (2014, 2015) investigated the flow velocity and turbulence characteristics in a staggered-boulder array in a typical fish pass, finding that the boulder array tended to increase the water depth and reduce the flow velocity. Compared with the flow around an isolated boulder, the wake region behind a boulder decayed slowly in the longitudinal direction and had the higher turbulent intensity and turbulent kinetic energy affected by neighbouring boulders. To further understand the effects of a boulder array, Baki *et al.* (2016) using a three-dimensional numerical model investigated the impacts of variations in boulder size, spacing, and pattern on flow characteristics. Sarkar *et al.* (2016) used double-averaging methodology (DAM) to successfully resolve the spatial heterogeneity in flows over a boulder array on a gravel bed. Sarkar (2016) found that turbulence characteristics vary insignificantly above the crest level of the array in comparison with those below the crest level. Also, macro-bed-roughness can result in the variability of the curve shape of the velocity profiles (Wang *et al.* 2015). Yager *et al.* (2007) found that boulders in a staggered pattern magnified the reach-averaged total bed shear-stress. Papanicolaou *et al.* (2011) found that the additional form drag created by the array produced a greater increase in reach-averaged total bed shear-stress compared with the isolated roughness conditions. Fang *et al.* (2017) investigated flows over submerged boulder arrays and found that boulder arrays promoted the local bed shear-stress distribution.

Boulders can promote the formation of discrete clusters, which serve as standalone anchor particles atop the finer particles and on the bed. The fine particles around boulders create a rough, permeable bed. Conventionally, turbulent flows over permeable beds are considered similar to those over impermeable beds since the effect of bed permeability on flows is usually considered negligible. However, when the flow is over a permeable bed, the surface and subsurface flow regions for a permeable bed exist above and within the bed, respectively. The flow over a permeable bed penetrates the bed, driving the exchange of mass, momentum, and energy between the bed surface and subsurface (Zippe & Graf 1983; Choi & Waller 1997; Liu *et al.* 2017). Bed permeability also controls flow mixing, encouraging a more organized near-wall flow structure and simultaneously governing flow physical processes within porous media (e.g. Cheng *et al.* 2011; Manes *et al.* 2011). It was observed that the von Karman constant over permeable beds is much lower than its standard value (=0.41) for terms of permeable smooth and rough beds (Breugem *et al.* 2006). Manes *et al.* (2009, 2011) found that bed permeability could enhance the wall-normal fluctuating velocity. This enhancement led to an increase in turbulent shear-stresses and thus further induced higher friction factors over permeable beds.

The fact is that numerous studies have reported hydrodynamics of boulder flows, and turbulent flow structure over permeable beds has been extensively investigated. However, the impact of the bed permeability on flows deflected by boulders has rarely been documented. This may lead to a knowledge gap between existing open channel flow theory and realistic flow configurations. Therefore, the present study designs a novel complex porous bed configuration, which describes flow propagating through a boulder array placed on a permeable bed. This study aims to investigate the impacts of the coexistence of boulders and bed permeability on the hydrodynamics. The investigated parameters are mean flow velocity distribution, Reynolds stresses and turbulent kinetic energy (TKE). To deepen the understanding of the interaction mechanism between flow, boulder and bed permeability, we further conduct a quadrant analysis of the turbulence structure, indicating the features of coherent structure over the permeable boulder-array bed. Finally, the budget of TKE is shown to describe the transfer of TKE by different mechanisms.

EXPERIMENTS AND METHODS

Experiments were carried out in a rectangular flume equipped with a recirculation system. The flume was 0.5 m wide, 0.6 m deep, and 16 m long with a streamwise bed slope of 0.1%. The flume commenced with a head tank,

capably filtering large-scale eddies and providing a smooth flow. The incoming flow was adjusted by an inlet valve to produce various flow configurations and the flow discharge was measured by a sharp-crested weir. The smooth bed (SB) was configured with a layer of glass beads with a constant diameter of $d_b = 14$ mm to mimic the gravel bed configuration, which is commonly observed in mountain river systems. Using glass beads packed in multiple layers to function as a permeable bed can refer to the setup of Manes *et al.* (2009), in which the bead diameter is 12 mm. Because of the one-layer set up, the bed with one-layer of beads is referred to as the impermeable bed (IMPB). To simply construct the permeable configuration, the second layer of beads was well packed on the IMPB, which was able to enhance the vertical motion of flows. Thereafter, it is referred to as the permeable bed (PB) in the current study.

Representing a natural boulder array, spherical plastic balls of a diameter of $D = 40$ mm were initially glued atop the PB in a staggered pattern (Figure 1(a)). The ball shape and dimension were designed similarly to other studies of flow around boulders (Papanicolaou *et al.* 2012; Liu *et al.* 2017). In total 55 boulders were arranged in 22 rows and each row includes either two or three boulders. The transverse spacing between two neighbouring boulders was set equal to the streamwise spacing between the centres of two neighbouring boulders (Figure 1(b)). This arrangement resulted in an aerial density of the boulder array of ~4.7%. Unlike other studies (Papanicolaou *et al.* 2012; Tsakiris *et al.* 2014), where boulders were directly placed atop the glass bead layer, boulders in this study were buried in glass-bead beds (Figure 1(c) and 1(d)). This treatment can provide a better description of natural scenarios of boulders and the neighbouring small-size particles (e.g. pebbles and gravels). In this sense, the boulders were exposed with different heights from the top of the bead layer (Figure 1(c)). The exposure height of the boulder can be simply defined as the difference (D_1) between the boulder and bead layers, as described in Figure 1(c). The state of boulders, therefore, can be completely exposed, slightly buried and largely buried. The exposure height, correspondingly, is $D_1 = D$, $D - d_b$ and $D - 2d_b$.

The flow velocities and turbulence quantities were obtained from the measurement of 3D instantaneous flow velocities using a SonTek®10 MHz type Acoustic Doppler Velocimeter (ADV). The sampling frequency was set at

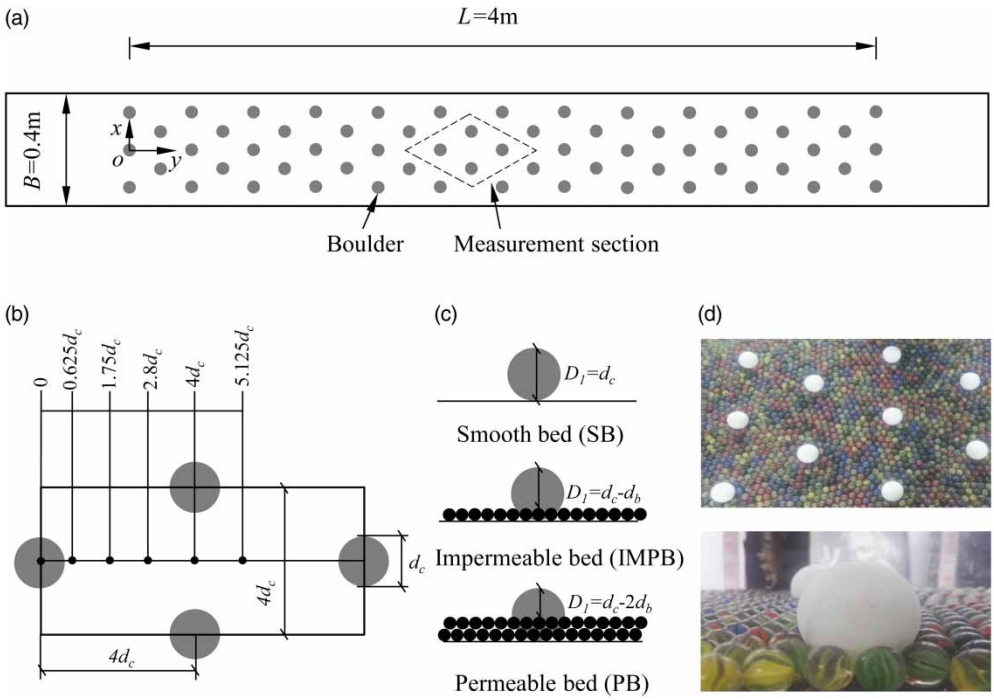

Figure 1 | (a) Plan view of the experimental set up of the boulder array; (b) sampling positions around a unit of boulders in the measurement section; (c) sketch of boulders placed on different bed configurations (i.e. SB, IMPB and PB); (d) real photograph of experiments for reference.

30 Hz. Within a sampling duration of 70 seconds, 2,100 points can be recorded so that the turbulent characteristics around a boulder can be well measured. The ADV used was able to measure flow velocities in a range of 0.001 m/s–5 m/s, with an accuracy of ±1%. To improve the data quality, those data with a ratio of signal to noise less than 70% were removed. In addition, high instantaneous velocity spikes were filtered to further refine the quality of the measured velocity data, using the phase-space thresholding technique proposed by Goring & Nikora (2002). Due to the employment of the one-point-measurement ADV, the measurement efficiency was not as high as with other velocity profilers such as ADV profiler and particle image velocimetry (PIV). For each run, measurements were carried out at every 1 cm across the entire water depth. This measurement resolution is similar to the setup of Nepf & Vinoni (2000), who used a one-point-measurement ADV to measure flow velocities controlled by near-canopy-top coherent structure. Under this resolution, a good analysis of the TKE budget depending on the spatial derivatives was made.

Two flow discharges, i.e. $Q = 28$ L/s and 48 L/s, were specified and a constant flow depth was maintained by an adjustable tailgate located at the exit of the flume, thus resulting in two Reynolds numbers (Re = 51,638 and 88,523). Therefore, the experiments are referred to as the low-rate and high-rate flows, respectively (Table 1). In experiments, the effective depth $h = h_o + z_o$, the distance from the water surface to the zero-velocity plane, where $z_o = 0.25d$ is the displacement position and h_o is the distance from the water surface to the top level of the glass beads. As shown in Figure 1(a), the test section has a length of 4 m located at 5 m downstream of the flume inlet to ensure a fully developed flow before entering the boulder array, and this can be confirmed by pre-experiments (examining the water depth). This is also similar to the setup of Papanicolaou *et al.* (2012) using similar geometry. The velocity measurement was conducted in the region where the flow became developed after moving through the boulder array. In the longitudinal direction, the test section started at a distance of 2 m from the most upstream test section and extended up to 2.205 cm (the ending vertical is located $5.125D$ downstream of the centre of the boulder). Along the distance of $5.125D$, five verticals ($0.625D$, $1.75D$, $2.8D$, $4D$ and $5.125D$) were measured.

RESULTS AND DISCUSSION

Time-averaged velocity

Figure 2 shows time-averaged streamwise and vertical velocities normalized by the shear velocity (u/u_*) for an IMPB (one-layer beads) and PB (two-layer beads) without a boulder array for the high-rate flow. The presentation firstly provides a basic understanding of the flow behaviour over an IMPB and PB. It is observed that the difference in the streamwise velocity was relatively small (Figure 2). For a PB of the high-rate case, the time-averaged velocity

Table 1 | Hydraulic conditions for the experiments

Run	Q (L/s)	Boulder size (mm)	Bead size (mm)	Layers of glass beads	Depth H (mm)	U_d (m/s)	u_* (m^2/s^2)	Reynolds number $Re = U_dH/\upsilon$	f
1	28	–	14	1	104	0.54	0.0319	51,638	0.00348
2	28	–	14	2	106	0.527	0.0323	51,638	0.00374
3	28	40	–	–	122	0.46	0.0345	51,638	0.00563
4	28	40	14	1	123	0.455	0.0347	51,638	0.00584
5	28	40	14	2	126	0.444	0.0351	51,638	0.00625
6	48	–	14	1	126	0.762	0.0351	88,523	0.00213
7	48	–	14	2	126	0.763	0.0351	88,523	0.00212
8	48	40	–	–	170	0.564	0.0408	88,523	0.00523
9	48	40	14	1	158	0.609	0.0393	88,523	0.00416
10	48	40	14	2	160	0.6	0.0396	88,523	0.00436

Notes: H = the effective depth; Re is the bulk Reynolds number; bed shear velocity $u_* = \sqrt{gHS}$, U_d = depth-averaged velocity; friction factor, flow resistance coefficient $f = (u_*/U_d)^2$.

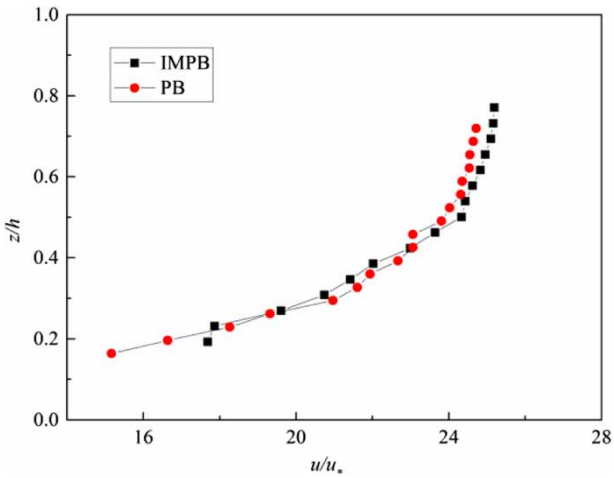

Figure 2 | The time-averaged streamwise velocities normalized by the shear velocity (u/u_*) for the IMPB and PB without a boulder array.

decreases by ~$0.8u_*$ and bulk flow resistance increases by ~4% (Table 1). The performance of streamwise velocity and bulk flow resistance for IMPB and PB is similar to the observation of Zippe & Graf (1983) and Manes *et al.* (2009).

Figure 3 shows the vertical distribution of streamwise velocity in regards to different bed configurations. Firstly, the time-averaged velocity at different locations downstream of a boulder is shown in Figure 3(a)–3(d). Generally compared with the IMPB, the averaged flow velocity above the PB downstream of the boulder ($x/D = 0.625$–5.125) is greater by roughly $0.4 \sim 1u_*$. The increase of the friction factor, however, was 5% and 7% for $Q = 48$ L/s and $Q = 28$ L/s, respectively (Table 1). Due to the different layers of glass beads laid on the bed, the magnitude of the streamwise velocities can be observed shifted upward as the layer number increases for both low-rate and high-rate flows (Figure 3(e) and 3(f)). However, the maximum velocities for the three bed configurations hold no significant difference. This indicates that the exposure height of boulders might have only a small impact on the mean streamwise velocities. It should be noted that as the bead layer number decreases, the variation rate in velocity near the boulders becomes larger. This is attributed to the boulders deflecting the near-bed velocity more as the exposure height increases. Interestingly, the deflection in velocity is more significant for the low-rate case. The possible cause is that for the high-rate case, vortices generated around the boulders might facilitate the exchange of flow momentum between the lower and upper flows. For the vertical velocity, the distributions for the SB and IMPB have similar profiles with no shift of distance observed even if a layer of beads is present for the IMPB. However, for the PB a clear upward shift of the profile can be observed. It can be noted that as the number of bead layers increases, the magnitude of the vertical velocity tends to decrease in the near-bed region. This might be because the presence of bed permeability may weaken the vertical flow motion by providing more pores for mass flux (Manes *et al.* 2009).

Turbulence intensities

Figure 4(a)–4(d) shows the streamwise turbulence intensity normalized by the shear velocity for the PB with a boulder array, compared with an exponential decay function [$u_{rms}/u_* = 2.3 \exp(-z/h)$] in regards to open channel flows reported by Nezu & Nakagawa (1993). Downstream of the boulders, u_{rms}/u_* is greater in the near-bed region and then decreases with increasing height. Different from the predictions of Nezu & Nakagawa (1993), the presence of the boulder array leads to a shift of the maximum of u_{rms}/u_* away from the bed. The position of the maximum value for both discharges is above the top of the boulders ($z/h = 0.2$–0.3). This is attributed to the generation of vortices triggered by the boulders deflecting the flow, which are consistent with the observations of Papanicolaou *et al.* (2012) and Baki *et al.* (2015). Originating from the boulder ($x/D = 0.625$), the magnitude of the turbulence intensity does not differ much as the measurement location is moved downstream far away from the boulder. This might suggest that the vortices are maintained in the current boulder spacing. For both the IMPB and PB of the low-rate case, the vertical profile of u_{rms}/u_* has a similar shape to the exponential decay function, but the magnitudes are slightly smaller, consistent with Papanicolaou *et al.* (2012). For the high-rate case, after the turbulence intensity reaches its maximum above the boulder, the magnitude decays more rapidly with the vertical distance than that for the PB. This results in a greater deviation between the measured profiles and the original exponential decay function.

The impacts of different bed configurations on both streamwise (Figure 4(e) and 4(f)) and vertical (Figure 4(g) and 4(h)) turbulence intensities at $x/D = 0.625$ are illustrated.

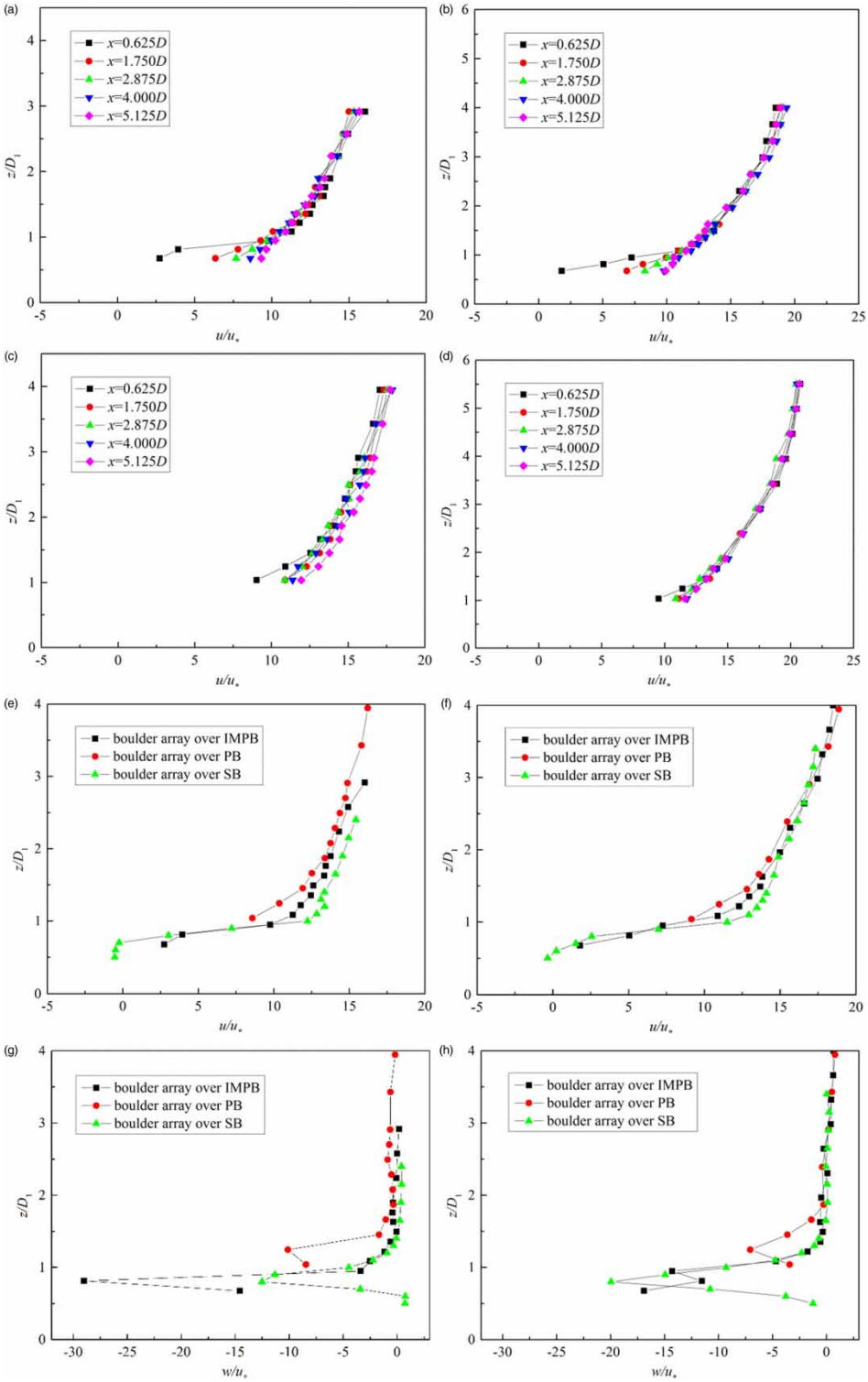

Figure 3 | Distribution of streamwise velocity. (a) Low-rate flow and (b) high-rate flow for the PB with a boulder array, and for (c) low-rate flow and (d) high-rate flow for the IMPB with a boulder array. Streamwise velocity for different bed configurations for (e) low-rate flow and (f) high-rate flow. Vertical velocity over different bed configurations for (g) low-rate flow and (h) high-rate flow.

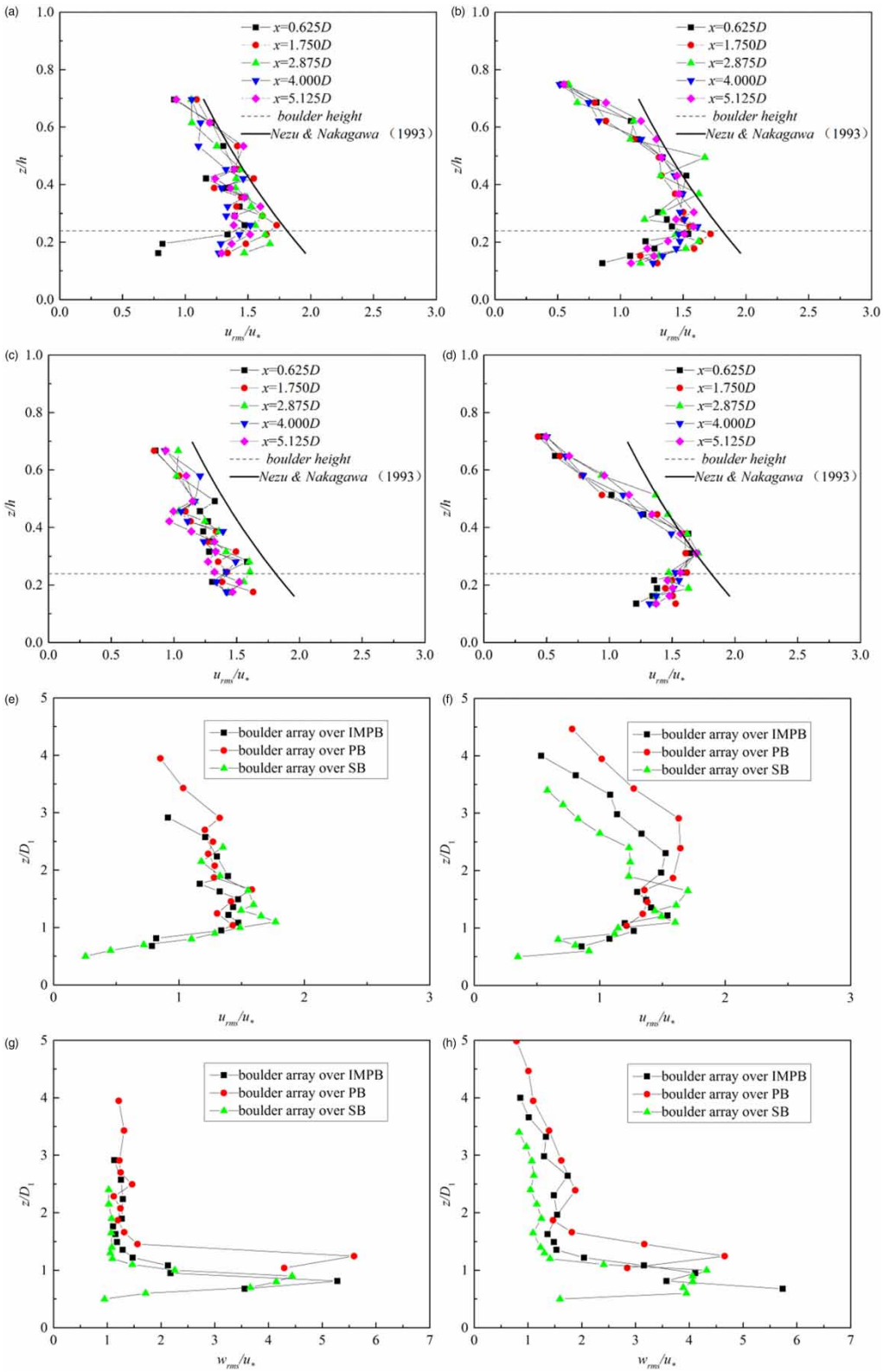

Figure 4 | Turbulence intensities at $x/D = 0.625$ for different bed configurations: (a, c, e, g) for the low-rate flow and (b, d, f, h) for the high-rate flow.

Herein, z/D_1 is taken as the y-axis to suggest the impact of the boulders on flows. Therefore, $z/D_1 = 1$ indicates the top of the boulders for the IMPB and PB. The distribution of u_{rms}/u_* has a negligible difference for the low-rate flow. However, for the high-rate flow, the near-bed peak of u_{rms}/u_* exhibits an apparent upward shifting off the boulder level as the bead layer increases. However, the similar magnitude and decay ratio for different bed configurations suggest a similar level of generated turbulence. The upward shifting is also identified in regards to w_{rms}/u_*. The effect is apparent for the low-rate flow, which is different from u_{rms}/u_*. This upward shifting of turbulence might be attributed to different patterns of vortices shedding from the boulders with different bed permeabilities, which needs to be further studied.

TKE budget

The analysis of the TKE budget can account for how the flow structure, particularly near the bed, is affected by different turbulence mechanisms. This can allow us to further understand the impact of the bed permeability on the boulder bed. The budget of the TKE (defined as $k = 0.5(u_{rms}^2 + v_{rms}^2 + w_{rms}^2)$) can be conducted by analysing the transport equation of the TKE. The transport equation, assuming the flow as being steady and the vertical flow motion negligible, involves the production (T_p), dissipation (e), turbulent diffusion (T_D), pressure energy diffusion (P_D) and viscous diffusion (V_D). Therefore, the TKE transport equation reads:

$$\frac{Dk}{Dt} = 0 = T_p + T_D + P_D + V_D + e \tag{1}$$

where $T_p = -\overline{u'w'}(\partial u/\partial z)$, $T_D = \partial(\overline{kw'})/\partial z$, $V_D = -\nu\partial^2 k/\partial z^2$.

The dissipation term (e) is not determined from the velocity measurement since this term involves the second-order correlation of the fluctuating velocities. An alternative approach to estimating e is by fitting the spectra of the longitudinal velocity in the inertial sub-range according to Kolmogorov's $-5/3$ theory as below (Baki *et al.* 2015):

$$S(f) = C(2\pi)^{-2/3}u^{2/3}e^{2/3}f^{-5/3} \tag{2}$$

where $S(f)$ is the power spectra of the streamwise velocity in the frequency domain, f is the frequency, and C is a non-dimensional constant with a value of 0.52. Among the above terms, the instantaneous pressure cannot be directly measured by the velocity field, so the pressure transport can be obtained by the residual of the other total terms, yielding:

$$P_D \approx R = T_p - T_D - V_D - e \tag{3}$$

Figure 5 depicts $S(f)$ in the near-bed region ($z/h = 0.2$) and compares the boulder wake at this point for the high-rate flow downstream of the boulder ($x/D = 0.625$ and 4).

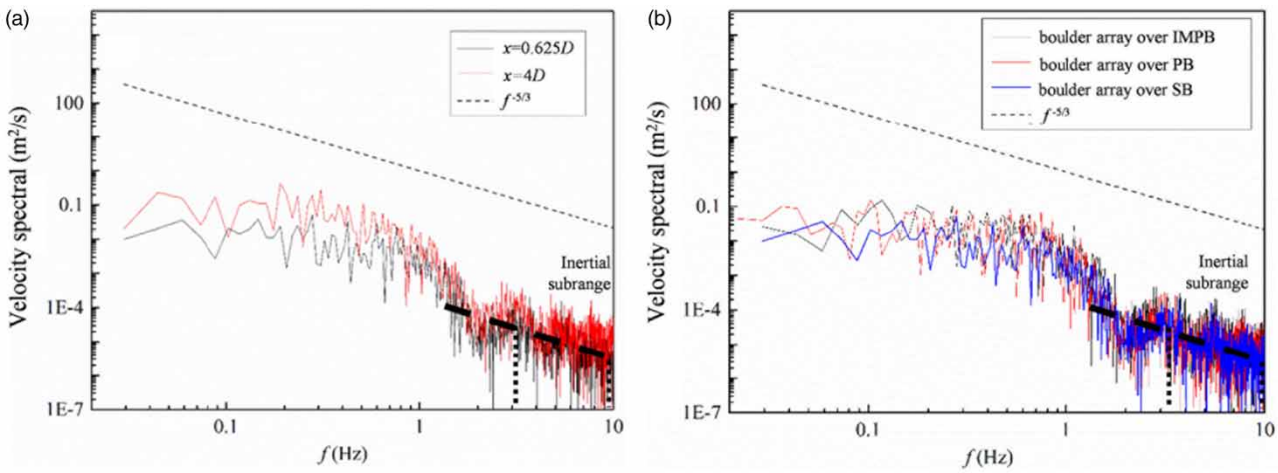

Figure 5 | Power spectral density of the streamwise velocity at $z/h = 0.2$ (a) at different x/D and (b) for different bed configurations.

With plenty of fluctuations in the spectra within a boulder array for the SB, IMPB and PB, the range of the frequency could be fitted with a −5/3 slope line, reducing the confidence level of the line. However, the overall energy of the flow downstream of the boulder was very similar to the IMPB and PB. As with the flow over the PB, the turbulence continuously dissipates by penetrating into the permeable bed, like a low-pass filter (Manes *et al.* 2009). Thus, the gap between the IMPB and PB becomes small in the inertial sub-range. The data fitted the least-squares in the range shown to be parallel to a −5/3 slope. Therefore, the dissipation rate (e) was estimated using Equation (2).

Figure 6 shows the TKE budget immediately downstream of the boulder ($x/D = 0.625$) for the IMPB and PB. Similar to the distribution of the turbulence intensity (Figure 4), the TKE just above the boulder top prevails over other locations far away from the boulder top. It is clearly noted that the production term (T_P) plays a significant role in the generation of the TKE for different bed configurations and discharges. Interestingly, the pressure diffusion term (P_D) as the residual of all other terms behaves comparably to T_P. The turbulent diffusion (T_D) and dissipation (e) hold the function of the decay of the TKE, thus being negative. It should be noted that the dissipation (e) is greater when approaching the glass bead layer. This suggests that the generated vortices diminish in the near-bed region. The turbulent diffusion is small, indicating that the effect of vortices is insufficient to redistribute the TKE. For the high-rate case, every component to determine the TKE is greater than that for the low-rate case despite the

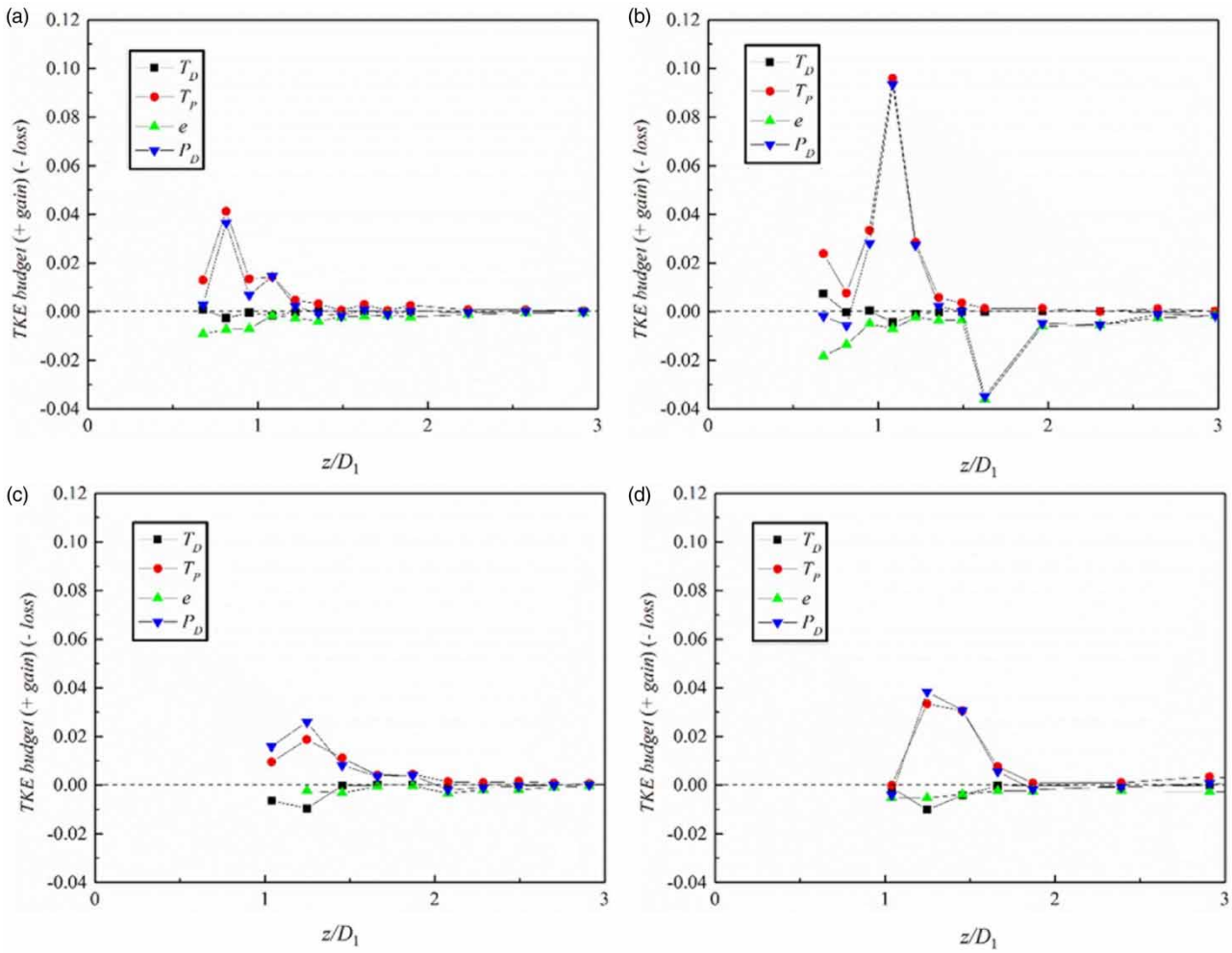

Figure 6 | TKE budget at $x/D = 0.625$ over (a) the IMPB for the low-rate flow, (b) the IMPB for the high-rate flow, (c) the PB for the low-rate flow and (d) the PB for the high-rate flow.

presence of bed permeability. The bed permeability seems to have negative impacts on all terms of the TKE budget. Specifically, the magnitude of all terms is smaller for the PB than for the IMPB. However, the cause might be uncertain since the bed permeability (increasing bead layers) leading to a decrease in exposure height of the boulders might also decrease turbulent activity near the boulders. Another interesting observation is that the presence of the bed permeability tends to shift the maximum values of some terms a small distance away from the boulder top. This is consistent with the distribution of turbulence intensities (Figure 4).

Quadrant analysis of turbulence structure

To analyse the characteristics and contributions of both the burst and sweep events on the turbulence, we used quadrant analysis to examine the conditional statistics of the velocity fluctuations. As suggested by Lu & Willmarth (1973), a hole-size parameter H was defined in the $u'w'$ plane to determine the dominant instantaneous Reynolds stress, enclosed by four curves $|u'w'| = H\overline{u'w'}$. Depending on the selected hole size, this relationship can clearly distinguish between strong and the weak events. The contributions of a particular quadrant to the Reynolds shear-stress is given as:

$$S_{i,H} = \frac{u'w'_i}{\overline{u'w'}} = \frac{1}{\overline{u'w'}} \lim \frac{1}{T} \int_0^T u'w' I_{i,H}(t)dt \tag{4}$$

where T is the sampling time and $I_{i,H}$ is the detection function giving:

$$I_{i,H} = \begin{cases} 1 & \text{when} |u'w'(t)|_i \geq H\overline{u'w'} \\ 0 & \text{otherwise} \end{cases} \tag{5}$$

Four events can be described by the above equations, which are the events in the quadrants that were outward interactions, $Q1$ $(i = 1, \quad u' > 0, w' > 0)$; ejections, $Q2$ $(i = 2, \quad u' < 0, w' > 0)$; inward interactions, $Q3$ $(i = 3, u' < 0, w' < 0)$; and sweeps, $Q4$ $(i = 4, u' > 0, w' < 0)$. Quadrant analysis was made for $H = 0$ and 2, respectively. This aims to investigate the contribution of high-frequency small eddies (for $H = 0$) and low-frequency large vortices (for $H = 2$) (Balachandar & Bhuiyan 2007).

Since the $Q2$ and $Q4$ represent the dominant events of turbulence and carry the major mass, momentum and energy during the velocity fluctuations, hereby we only present the results of the $Q2$ and $Q4$ as shown in Figure 7(a)–7(d) for $H = 0$ and Figure 7(e)–7(h) for $H = 2$. For comparison, the results for bed configurations without the boulder array are firstly presented before that for boulder bed. For $H = 0$, without a boulder array, the near-bed $Q4$ dominates the entire turbulent activity compared with the $Q2$ (Figure 7(a) and 7(b)). This indicates that the downward sweeps are the major process in transporting the turbulence momentum and energy from the outer flow to the inner flow. However, the presence of the bed permeability seems to have negligible impact on the magnitude of $Q2$ and $Q4$, except for a short downward shifting of the maximum of $Q2$ and $Q4$. This identity is somewhat consistent with the distribution of turbulence intensity (see Figure 4). The short shifting might be from the bed porosity providing the extra space so that the $Q4$ event of turbulence can penetrate the deeper layer.

As the boulder array occurs, the near-bed $Q2$ behaves comparably to the $Q4$, suggesting that the turbulence momentum and energy exchange are driven equally by the ejections and sweeps. Even for the SB, the $Q2$ prevails over the $Q4$. Clearly, the presence of the glass beads appears to inhibit the generation of the $Q2$ and $Q4$ events. The magnitude of both turbulent events for the SB approximates 5–7 times those for the IMPB and PB. The increase in the glass bead layer also holds a similar but slight inhibiting effect. This suggests that the bed porosity may absorb the turbulent energy of the near-bed energy. However, the decrease in exposure height of the boulders may be the second cause of the weak turbulent activity when the glass bead layers exist. The presence of the bead layer somehow decreases the roughness of the bed configuration, thus weakening the turbulence.

As some small random fluctuating flow motions are filtered out (by setting $H = 2$), the $Q2$ for cases without the boulder array becomes significant, even exceeding the effect of $Q4$, and the $Q4$ is highly reduced compared with the values with respect to $H = 0$. This may be because the ejections ($Q2$) are dominated by low-frequency large eddies while the sweeps ($Q4$) are mainly assembled by high-frequency small eddies. With the filtering of small eddies, the large eddies take the major role. However, this change is not applicable to

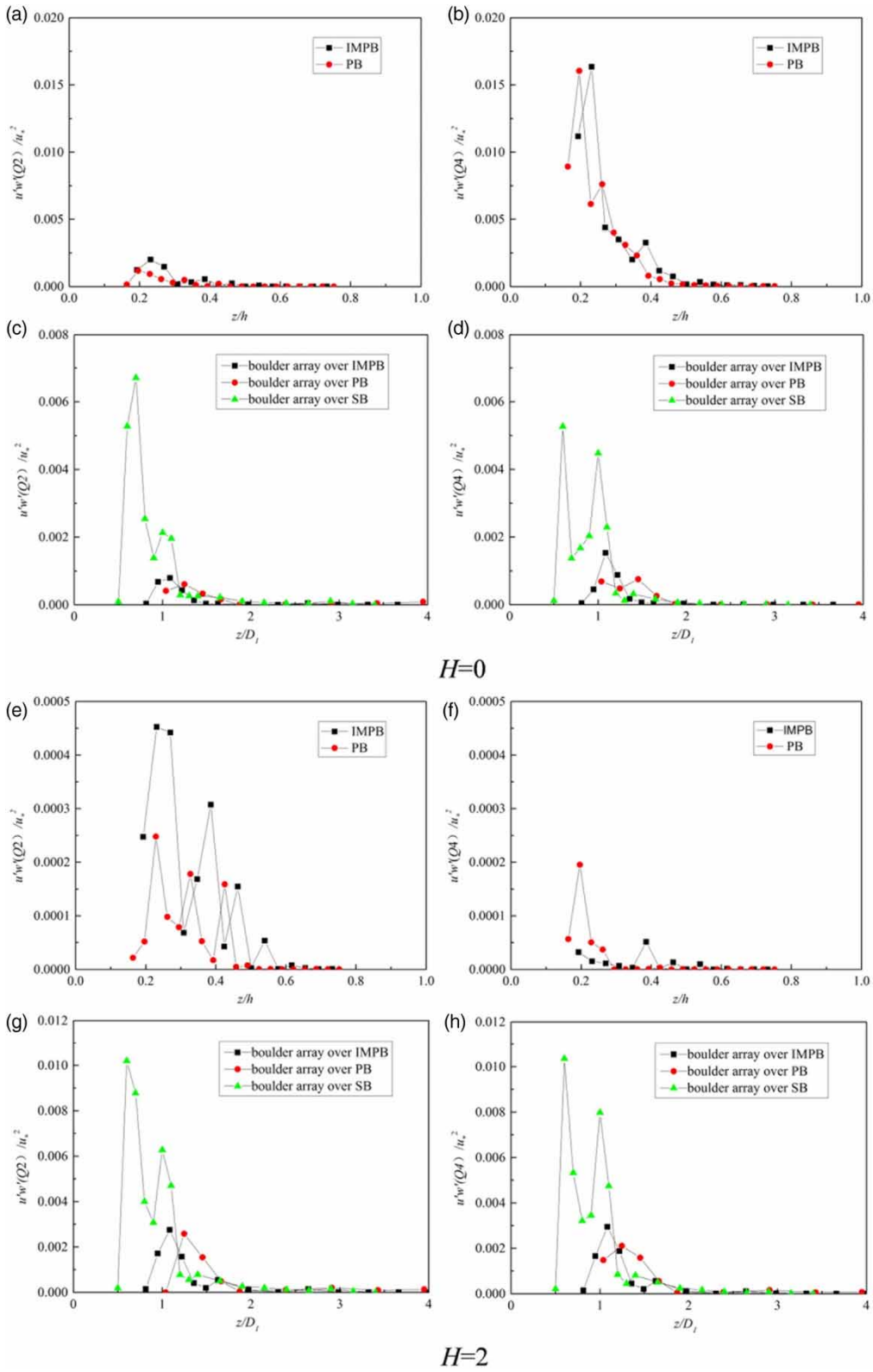

Figure 7 | Contribution of different quadrant events to the Reynolds stress for flow over different bed configurations for the high-rate flow case: (a–d) for $H = 0$ and (e–h) for $H = 2$.

the boulder bed configuration. By setting $H = 2$, the distribution and magnitude are still similar to those in the case of no boulder array. This suggests that the presence of the boulders is the main cause of the near-bed large eddies.

CONCLUSION

To address the impacts of the coexistence of boulders and bed permeability on flow characteristics, this study designed an array of boulders (simulated by plastic spherical balls) placed within well-packed glass-bead-made permeable beds. The instantaneous flow velocities were measured to achieve mean flow and turbulence characteristics to investigate those impacts. For background reference, hydrodynamics investigation was made over smooth beds (SB) with the boulder array. The major flow characteristics such as mean flow velocity, turbulence intensity, turbulent kinetic energy (TKE) and instantaneous Reynolds stresses (through quadrant analysis) were presented in this study. The results show that the increase in bed permeability through decreasing the exposure height of boulders has little impact on the magnitude of streamwise velocity, but the near-bed velocity gradient seems to decrease, indicating the reduction of the bed shear-stress. Similarly to the previous studies, it is identified that bed permeability enables the downward shifting of the peak of turbulence intensity probably due to the absorption of the turbulence momentum and energy. The TKE budget analysis shows that bed permeability tends to weaken production, transport and diffusion intensities of the TKE. With bed permeability increasing (or the exposure height of the boulders decreasing), the peaks of all TKE terms shift upward off the boulder top. However, the TKE budget through the entire depth cannot attain equilibrium. Finally, the quadrant analysis of turbulence structure, by setting different hole sizes, clearly reveals that the ejections ($Q2$) and sweeps ($Q4$) with and without the boulder array are dominated by turbulence structure of different scales.

ACKNOWLEDGEMENTS

This research was supported by the National Key R&D Program of China (2017YFC1502504 and 2018YFC150540203) and the National Natural Science Foundation of China (51639007, 51909178, and 41771543).

REFERENCES

Afzalimehr, H., Maddahi, M. R., Naziri, D. & Sui, J. 2019 Effects of non-submerged boulder on flow characteristics – a field investigation. *International Journal of Sediment Research* **34** (2), 136–143.

Baki, A. B. M., Zhu, D. Z. & Rajaratnam, N. 2014 Mean flow characteristics in a rock-ramp-type fish pass. *Journal of Hydraulic Engineering* **140** (2), 156–168.

Baki, A. B. M., Zhu, D. Z. & Rajaratnam, N. 2015 Turbulence characteristics in a rock-ramp-type fish pass. *Journal of Hydraulic Engineering* **141** (2), 04014075.

Baki, A. B. M., Zhu, D. Z. & Rajaratnam, N. 2016 Flow simulation in a rock-ramp fishpass. *Journal of Hydraulic Engineering* **142** (10), 04016031.

Balachandar, R. & Bhuiyan, F. 2007 Higher-order moments of velocity fluctuations in an open channel flow with large bottom roughness. *Journal of Hydraulic Engineering* **133** (1), 77–87.

Breugem, W. P., Boersma, B. J. & Uittenbogaard, R. E. 2006 The influence of wall permeability on turbulent channel flow. *Journal of Fluid Mechanics* **562**, 35–72.

Cheng, P. D., Li, L., Tang, J. & Wang, D. Z. 2011 Application of time-varying viscous grout in gravel-foundation anti-seepage treatment. *Journal of Hydrodynamics* **23** (3), 391–397.

Choi, C. Y. & Waller, P. M. 1997 Momentum transport mechanism for water flow over porous media. *Journal of Environmental Engineering* **123**, 792–799.

Dey, S., Sarkar, S., Bose, S. K., Tait, S. & Castro-Orgaz, O. 2011 Wall-wake flows downstream of a sphere placed on a plane rough wall. *Journal of Hydraulic Engineering* **137** (10), 1173–1189.

Euler, T., Herget, J., Schlömer, O. & Benito, G. 2017 Hydromorphological processes at submerged solitary boulder obstacles in streams. *CATENA* **157**, 250–267.

Fang, H. W., Liu, Y. & Stoesser, T. 2017 Influence of boulder concentration on turbulence and sediment transport in open-channel flow over submerged boulders. *Journal of Geophysical Research: Earth Surface* **122**, 2392–2410.

Goring, D. G. & Nikora, V. I. 2002 Despiking acoustic doppler velocimeter data. *Journal of Hydraulic Engineering* **128** (1), 117–126.

Lawless, M. & Robert, A. 2001 Scales of boundary resistance in coarse-grained channels: turbulent velocity profiles and implications. *Geomorphology* **39** (3-4), 221–238.

Liu, Y., Stoesser, T., Fang, H., Papanicolaou, A. & Tsakiris, A. G. 2017 Turbulent flow over an array of boulders placed on a rough, permeable bed. *Computers & Fluids* **158**, 120–132.

Lu, S. S. & Willmarth, W. W. 1973 Measurements of the structure of the Reynolds stress in a turbulent boundary layer. *Journal of Fluid Mechanics* **60** (3), 481–511.

Manes, C., Pokrajac, D., McEwan, I. & Nikora, V. 2009 Turbulence structure of open channel flows over permeable and impermeable beds: a comparative study. *Physics of Fluids* **21**, 125109.

Manes, C., Poggi, D. & Ridolfi, L. 2011 Turbulent boundary layers over permeable walls: scaling and near-wall structure. *Journal of Fluid Mechanics* **687**, 141–170.

Nepf, H. M. & Vivoni, E. R. 2000 Flow structure in depth-limited, vegetated flow. *Journal of Geophysical Research* **105**, 28547–28557.

Nezu, I. & Nakagawa, H. 1993 *Turbulence in Open-Channel Flows*. IAHR Monograph Series, A. A. Balkema, Rotterdam, The Netherlands.

Papanicolaou, A. N., Dermisis, D. C. & Elhakeem, M. 2011 Investigating the role of clasts on the movement of sand in gravel bed rivers. *Journal of Hydraulic Engineering* **137** (9), 871–883.

Papanicolaou, A. N., Kramer, C. M., Tsakiris, A. G., Stoesser, T., Bomminayuni, S. & Chen, Z. 2012 Effects of a fully submerged boulder within a boulder array on the mean and turbulent flow fields: implications to bedload transport. *Acta Geophysica* **60** (6), 1502–1546.

Sadeque, M. A. F., Rajaratnam, N. & Loewen, M. R. 2009 Effects of bed roughness on flow around bed-mounted cylinders in open channels. *Journal of Engineering Mechanics* **135** (2), 100–110.

Sarkar, S. 2016 Time-averaged turbulent flow characteristics over a highly spatially heterogeneous gravel-bed. *Acta Geophysica* **64** (5), 1797–1824.

Sarkar, S., Papanicolaou, A. N. & Dey, S. 2016 Turbulence in a gravel-bed stream with an array of large gravel obstacles. *Journal of Hydraulic Engineering* **142** (11), 04016052.

Shamloo, H., Rajaratnam, N. & Katopodis, C. 2001 Hydraulics of simple habitat structures. *Journal of Hydraulic Research* **39** (4), 351–366.

Tsakiris, A. G., Papanicolaou, A. N., Hajimirzaie, S. M. & Buchholz, J. H. J. 2014 Influence of collective boulder array on the surrounding time-averaged and turbulent flow fields. *Journal of Mountain Science* **11** (6), 1420–1428.

Wang, X. K., Ye, C., Wang, B. J. & Yan, X. F. 2015 Experimental study on velocity profiles with different roughness elements in a flume. *Acta Geophysica* **63** (6), 1685–1705.

Yager, E. M., Kirchner, J. W. & Dietrich, W. E. 2007 Calculating bed load transport in steep boulder bed channels. *Water Resourses Research* **43**, W07418.

Zippe, J. H. & Graf, W. H. 1983 Turbulent boundary-layer flow over permeable and non-permeable rough surfaces. *Journal of Hydraulic Research* **21** (1), 51–65.

First received 28 December 2019; accepted in revised form 2 March 2020. Available online 18 March 2020